


Antiferromagnetic order in the layered magnetic topological insulator MnBi_2Se_4 probed by resonant soft x-ray scattering

Xiang Chen ^{1,2,*}, Alejandro Ruiz,³ Alexander J. Bishop,⁴ Brandon Gunn ³, Rourav Basak ³, Tiancong Zhu,² Yu He,^{5,2,1} Maya Vranas,³ Eugen Weschke,⁶ Roland K. Kawakami,⁴ Robert J. Birgeneau ^{2,1,7} and Alex Frano^{3,†}

¹Materials Science Division, Lawrence Berkeley National Lab, Berkeley, California 94720, USA

²Physics Department, University of California, Berkeley, California 94720, USA

³Department of Physics, University of California, San Diego, California 92093, USA

⁴Department of Physics, The Ohio State University, Columbus, Ohio 43210, USA

⁵Department of Applied Physics, Yale University, New Haven, Connecticut 06511, USA

⁶Helmholtz-Zentrum Berlin für Materialien und Energie, BESSY II, D-12489 Berlin, Germany

⁷Department of Materials Science and Engineering, University of California, Berkeley, California 94720, USA



(Received 17 August 2023; accepted 24 April 2024; published 9 May 2024)

The quasi-two-dimensional magnetic topological insulator MnBi_2Se_4 , stabilized via nonequilibrium molecular beam epitaxy, is investigated by resonant soft x-ray scattering. Kiessig fringes are observed, confirming a high sample quality and a thin film thickness of 10 septuple layers (~ 13 nm). An antiferromagnetic Bragg peak is observed at the structurally forbidden reflection, whose magnetic nature is validated by studying its temperature, energy, and polarization dependence. Through a detailed analysis, an A-type antiferromagnetic order with in-plane moments is implied. This alternative spin structure in MnBi_2Se_4 , in contrast to the Ising antiferromagnetic states in other magnetic topological insulators, might be relevant for hosting new topological states.

DOI: [10.1103/PhysRevB.109.184418](https://doi.org/10.1103/PhysRevB.109.184418)

I. INTRODUCTION

The newly uncovered axion insulator states with quantized magnetoelectric effects, Chern insulator phases, and quantum anomalous Hall effect with dissipationless chiral edge states in magnetic topological insulators, open the door for potential applications in next-generation spintronics and quantum computing [1–17]. The coupling of magnetism and topology is essential to support these exotic quantum topological states. The recently discovered quasi-two-dimensional (quasi-2D) van der Waals-bonded (vdW) compound MnBi_2Te_4 [10–12], in which the intralayer manganese (Mn) atoms within a septuple layer (SL) (i.e., Te-Bi-Te-Mn-Te-Bi-Te) are magnetically ordered, provides important opportunities to explore these rich magnetic topological states. As a close analog, the sister compound MnBi_2Se_4 is predicted to host either a nodal line with in-plane magnetic moments or a Weyl semimetal state with Ising spins [18,19], further highlighting the significance of magnetic interactions. Therefore, understanding the magnetic ground states in these materials is a prerequisite for further exploring new topological states.

The exploration of quantum topological states in the quasi-2D vdW magnet MnBi_2Se_4 is hindered by the extreme difficulty in single crystal synthesis. Efforts to synthesize bulk crystals of vdW MnBi_2Se_4 have only produced its monoclinic form [20,21], which is a thermodynamically more stable

phase. By using nonequilibrium molecular beam epitaxy (MBE) to stabilize the vdW layers, multilayer vdW MnBi_2Se_4 crystal films were recently synthesized [22,23]. Although magnetization measurements of the vdW MnBi_2Se_4 thin films suggest the existence of ferromagnetism with an ordering temperature ~ 10 K, as evidenced by the temperature-dependent magnetization and the out-of-plane hysteresis loops of the isothermal magnetization, an antiferromagnetic (AFM) order has also been implied [22]. Due to the limited volume of thin films (up to 20 SLs), neutron scattering studies of the magnetic properties of MnBi_2Se_4 are difficult. Because of the aforementioned challenges, the magnetic ground state of layered MnBi_2Se_4 remains elusive.

Resonant (elastic) soft x-ray scattering (RSXS) [24–28] offers a unique, element-specific probe to study spatial modulations of the spin degrees of freedom in solids on a nanoscopic length scale. However, soft x-rays are subject to strong absorption by ambient atmosphere and the penetration depth into a solid, single-crystalline material is on the order of a few to hundreds of nanometers, which means that surface effects may become relevant. Therefore, RSXS setups are designed and maintained under high vacuum conditions, which pose challenges for investigating magnetic systems at very low temperatures (below 20 K). Here, we demonstrate the applicability of utilizing the RSXS technique to investigate the bulk magnetic properties of a 10-SL MnBi_2Se_4 thin film sample (thickness ~ 13 nm). By tuning the x-ray energy $E = \hbar\omega$ to the Mn L_3 absorption edge, the photon-excited intermediate state is sensitive to the magnetic order via the dipole allowed Mn $2p \rightarrow 3d$ (L_3) transition involved in the resonant elastic scattering process [24,25]. Our study implies

*Present address: Sun Yat-Sen University, Guangzhou, China; chenx889@mail.sysu.edu.cn.

†afrano@ucsd.edu

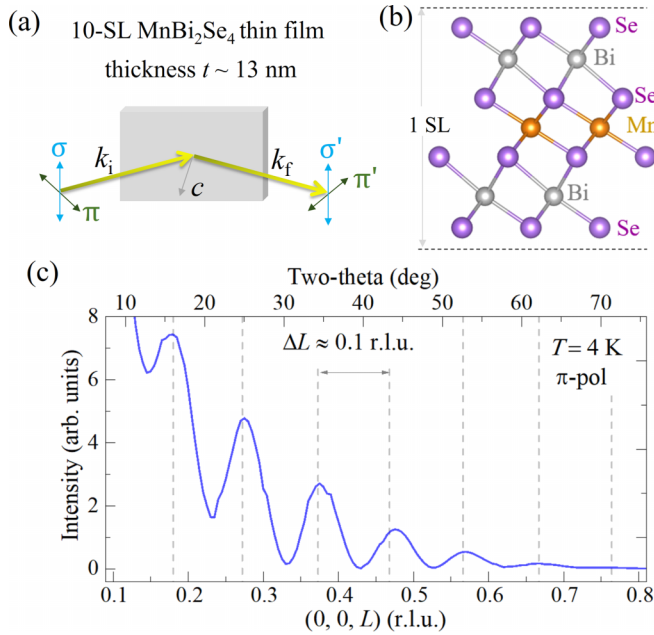


FIG. 1. (a) Schematic of the resonant soft x-ray scattering (RSXS) experiment on a 10-septuple-layer (10-SL) MnBi_2Se_4 thin film with a thickness of $t \approx 13$ nm. The lattice c direction lies within the horizontal scattering plane. The incoming x-ray can be either horizontally polarized (H pol or π pol) or vertically polarized (V pol or σ pol). (b) The atomic structure of one SL MnBi_2Se_4 . Colored atoms: Se (purple), Bi (gray), and Mn (orange). (c) Longitudinal L scan of the 10-SL MnBi_2Se_4 thin film at $T = 4$ K. Kiessig fringes [29,30] are evident with an average periodicity of $\Delta L = 0.1$ r.l.u., which is consistent with the sample thickness $t \approx 13$ nm. The corresponding two-theta angles are also labeled.

that the magnetic ground state of the quasi-2D vdW magnet MnBi_2Se_4 is an A-type AFM order below a Néel temperature $T_N \approx 9$ K.

II. EXPERIMENTAL RESULTS

Single-crystalline vdW MnBi_2Se_4 thin films were synthesized layer-by-layer using the MBE technique under nonequilibrium condition [22]. A 10-SL thick MnBi_2Se_4 film on Al_2O_3 (0001) with a ~ 5 nm selenium (Se) cap was prepared. The RSXS experiments were performed at the UE46_PGM-1 beamline at Helmholtz-Zentrum Berlin. A horizontal scattering geometry was utilized with the sample lattice c direction lying within the scattering plane [Fig. 1(a)] [26,31]. The Bragg peaks $\mathbf{Q} = (H, K, L) \cdot (\frac{4\pi}{\sqrt{3}a}, \frac{4\pi}{\sqrt{3}b}, \frac{2\pi}{c})$ are defined in reciprocal lattice units (r.l.u., the latter bracket) with lattice parameters $a = b \approx 4.0$ Å and $c \approx 12.8$ Å [22]. Here, for simplicity, the lattice constant c is defined as one SL thickness c_{SL} [Fig. 1(b)], instead of $3c_{\text{SL}}$ as in MnBi_2Te_4 . The x-ray scattering data are collected near the Mn L_3 edge to enhance the magnetic scattering signal [32–34]. The incoming x-rays can be either horizontally polarized (H pol or π pol) or vertically polarized (V pol or σ -pol), but the polarization of the scattered x-rays is not analyzed. Therefore, both outgoing σ' -pol and π' -pol channels contribute to the scattered intensity.

In general for a resonant x-ray scattering experiment, the scattering amplitude consists of both charge and magnetic scattering, and can be written as [24,25,28]

$$f = f_0(\mathbf{e}_\nu^* \cdot \mathbf{e}_\mu) - if_1(\mathbf{e}_\nu^* \times \mathbf{e}_\mu) \cdot \mathbf{m} + f_2(\mathbf{e}_\nu^* \cdot \mathbf{m})(\mathbf{e}_\mu \cdot \mathbf{m}), \quad (1)$$

in which f_0 , f_1 , and f_2 are the monopole, magnetic dipole (E_1), and quadrupole (E_2) part of the energy dependent resonance amplitude, respectively. \mathbf{e}_μ ($\mu = \sigma$ or π) and \mathbf{e}_ν ($\nu = \sigma'$ or π') are unit vectors along the polarization direction of the electric field component of the incident and out-going x-ray beams, respectively. \mathbf{m} is the unit vector along the spin direction. At the $3d$ transition metal L edges, the E_1 resonant scattering is often greatly enhanced. Meanwhile, by tuning the x-ray polarization and energy, as well as the scattering geometry, the charge scattering part can sometimes be much reduced, such that considering only the magnetic dipole term in Eq. (1) is sufficient for describing the resonant x-ray scattering intensity [28,31,35,36]. Thus, because of the large resonant magnetic scattering amplitude at the Mn L edges and the inversion symmetry at the Mn sites, the resonant magnetic scattering intensity at a structurally forbidden Bragg peak position can be approximated by including the linear resonant scattering amplitude in magnetic moment (without considering the charge scattering amplitude) [26–28,35,36],

$$I_{\mu\nu} \propto \left| \sum_j e^{i\mathbf{Q} \cdot \mathbf{r}_j} (\mathbf{e}_\mu \times \mathbf{e}_\nu^*) \cdot \mathbf{m}_j F(\mathbf{E}) \right|^2, \quad (2)$$

to first order in the magnetic moment \mathbf{m}_j of the ion located at site \mathbf{r}_j within the unit cell. $F(\mathbf{E})$ is the nonlocal, photon energy dependent scattering tensor. Since the polarization of the scattered light is not analyzed, the measured intensities are $I_H = I_\pi \equiv I_{\pi\sigma'} + I_{\pi\pi'}$ and $I_V = I_\sigma \equiv I_{\sigma\sigma'} + I_{\sigma\pi'}$. Also, since $\mathbf{e}_\sigma \parallel \mathbf{e}_{\sigma'}$, this obviously leads to $I_{\sigma\sigma'} = 0$, and leaves $I_\sigma = I_{\sigma\pi'}$.

The quasi-2D vdW magnet MnBi_2Se_4 is isostructural to MnBi_2Te_4 (space group $R\bar{3}m$), with covalently bonded SLs (i.e., Se-Bi-Se-Mn-Se-Bi-Se) as the base unit [Fig. 1(b)]. The atomic-scale structures of MnBi_2Se_4 were verified via scanning transmission electron microscopy, scanning tunneling microscopy, and atomic force microscopy, confirming the layered vdW structure, as opposed to the monoclinic form produced by single-crystal synthesis [22,23]. The soft x-ray scattering experiments were performed on a 10-SL MnBi_2Se_4 thin film sample. From the longitudinal L scan of the x-ray diffraction measurement [Fig. 1(c)], well defined Kiessig fringes [29,30] are evident with an average periodicity of $\Delta L = 0.1$ r.l.u., indicating a coherent interference of the x-ray beams reflected on the top cap layer of amorphous Se and the interface of MnBi_2Se_4 and Al_2O_3 (0001). The large oscillating amplitude of the Kiessig fringes at a low two-theta angle, as compared to the peak height of the charge/magnetic peak in Figs. 2 and 3, implies a small surface roughness of the films. Moreover, the thickness of the MnBi_2Se_4 film can be readily estimated as $t = \frac{2\pi}{\Delta L} = 10 c_{\text{SL}} \approx 13$ nm, which matches in excellent agreement with the targeted MBE film growth thickness of 10 SLs.

By tuning the x-ray energy to the Mn L_3 absorption edge ($E \approx 640$ eV) and slightly tilting the rocking angle off by 0.25° (Figs. S1 and S2, [37]), which suppress the Kiessig

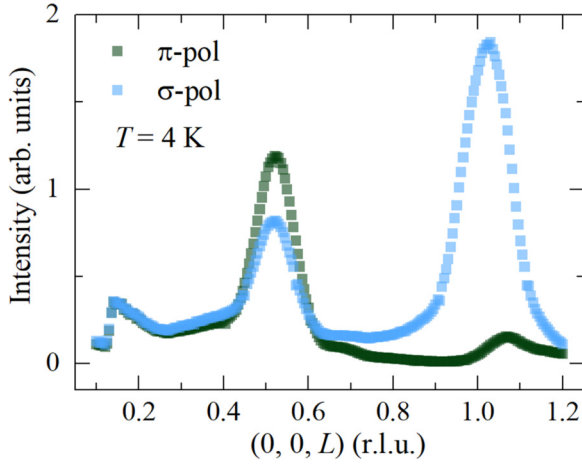


FIG. 2. Comparison of the longitudinal L scan at the Mn L_3 edge (energy $E = 640.2$ eV) at $T = 4$ K with two different polarizations of incoming x-rays: π pol (green) and σ pol (blue). With π -pol incoming photons, the structural Bragg peak $(0, 0, 1)$ is greatly suppressed; while the intensity of the magnetic Bragg peak $(0, 0, 0.5)$ is only moderately enhanced from σ pol to π pol. The intensity jump near $L = 0.15$ r.l.u. is an artifact.

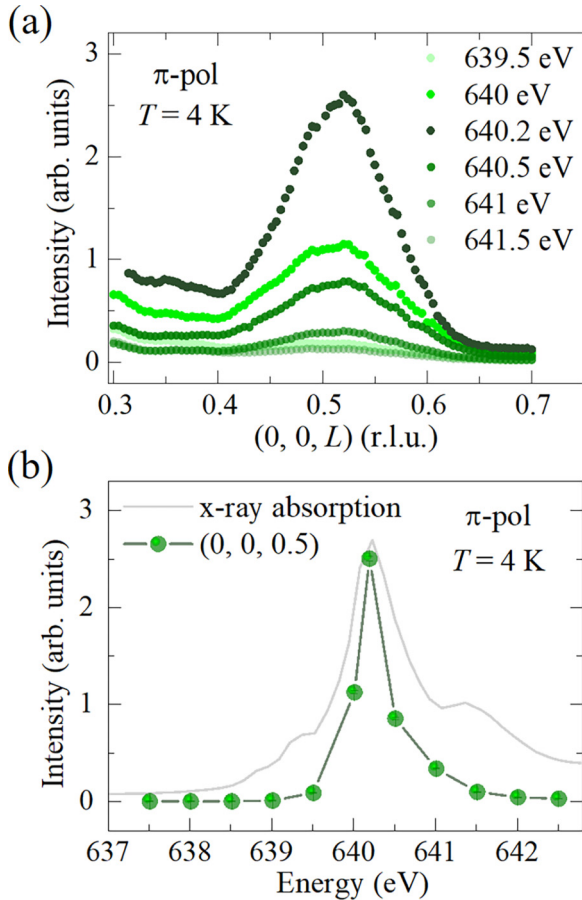


FIG. 3. Energy dependence of the $(0, 0, 0.5)$ peak at $T = 4$ K with π -pol incoming x-rays: (a) L scans of the $(0, 0, 0.5)$ peak at select energies near the Mn L_3 edge. (b) Energy dependence of the integrated area of the L scans of the $(0, 0, 0.5)$ peak (green circles). For comparison, the x-ray absorption data are also plotted (solid gray line).

fringes without affecting the magnetic signals, a Bragg peak is revealed at the structurally forbidden position $\mathbf{Q}_0 = (0, 0, 0.5)$ from the longitudinal L scan below the magnetic onset temperature (at $T = 4$ K), in addition to the structural Bragg peak at $\mathbf{Q}_1 = (0, 0, 1)$ (Fig. 2). The contrasting nature of the Bragg peaks \mathbf{Q}_0 and \mathbf{Q}_1 is apparent; opposing polarization dependent behavior is clearly observed when the polarization of the incoming x-rays is switched from σ pol to π pol (Fig. 2). The structural Bragg peak intensity at \mathbf{Q}_1 is greatly reduced with π -pol incoming x-rays, while the magnetic Bragg peak \mathbf{Q}_0 is only moderately influenced by varying the polarization of the incoming x-rays (Fig. 2). As discussed later, the stronger signal at \mathbf{Q}_0 for π pol is consistent with Mn moments oriented in-plane as opposed to out-of-plane, as observed in magnetization measurements [22].

To understand fully the nature of the \mathbf{Q}_0 peak, we present a further study of its dependence on x-ray energy and temperature. Figure 3 shows the photon energy dependence of the \mathbf{Q}_0 reflection, collected at 4 K with π -pol incident x-rays. The \mathbf{Q}_0 peak intensity shows a dramatic dependence on the photon energy. A single and sharp energy-dependent peak profile with an estimated peak width of ~ 0.6 eV is evident near the Mn L_3 edge, in which the maximum intensity of the \mathbf{Q}_0 reflection is recorded at $E = 640.2$ eV [green circles in Fig. 3(b)]. As a comparison, the x-ray absorption spectra at the Mn L_3 edge is also plotted [gray line in Fig. 3(b)]. This sharp resonance in photon energy is a strong signature of the magnetic nature of the \mathbf{Q}_0 reflection [26,27] because the resonant scattering proceeds in two stages, occurs in conjunction with an absorption edge, and the scattered intensity depends on both the incoming and outgoing photon polarizations.

The temperature dependence of the \mathbf{Q}_0 peak at the resonance energy ($E = 640.2$ eV) is also examined, as shown in Fig. 4. With increasing temperature, the \mathbf{Q}_0 peak intensity on resonance becomes vanishingly small above the magnetic transition temperature $T_N \approx 10$ K [Figs. 4(a) and 4(b)]. We argue that, from the polarization-, temperature-, and energy-dependent studies, the $\mathbf{Q}_0 = (0, 0, 0.5)$ Bragg peak in Figs. 2–4 is dominantly magnetic in nature, while the charge scattering contribution is greatly suppressed by tuning the polarization and the energy of the incident x-rays, as well as tilting the rocking angles (Figs. S1 and S2, [37]). This magnetic $(0, 0, 0.5)$ Bragg peak implies the AFM nature of the magnetic ground state in vdW MnBi_2Se_4 .

To gain more insight about the nature of the magnetic transition in MnBi_2Se_4 , a power law fitting of the order parameter squared [38–41]—the integrated peak intensity after subtracting the high-temperature background at $T = 12$ K—is employed at the magnetic reflection $\mathbf{Q}_0 = (0, 0, 0.5)$ under the form

$$I \propto |T_N - T|^{2\beta}. \quad (3)$$

The power law fit of the $\mathbf{Q}_0 = (0, 0, 0.5)$ magnetic peak yields $T_N = 9(1)$ K and $\beta = 0.37(4)$ [Fig. 4(b)]. The fitted value $T_N = 9(1)$ K, reflecting a bulk magnetic transition, is consistent with the temperature estimated from magnetization data. It is worth mentioning that the $\beta = 0.37(4)$ value is consistent, within the range of errors, with that of MnBi_2Te_4 , which is $\beta = 0.32(1)$ or $0.35(2)$, determined from neutron diffraction experiments [42,43].

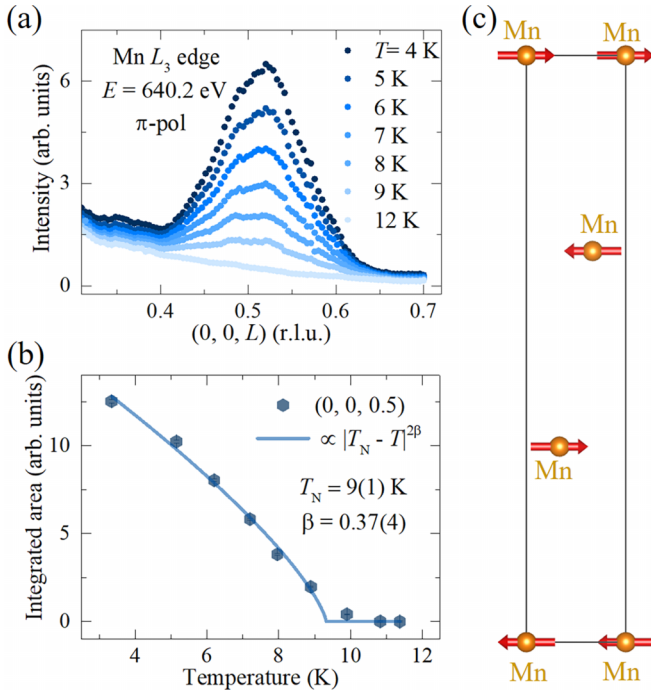


FIG. 4. Temperature dependence of the $(0, 0, 0.5)$ peak on resonance (at $E = 640.2$ eV), collected with π -pol incoming x-rays: (a) L scans of the $(0, 0, 0.5)$ peak at select temperatures. The peak intensity is completely suppressed at $T = 12$ K. (b) Temperature dependence of the integrated area of the $(0, 0, 0.5)$ peak. The solid blue line is a power law fit to the data with a form: $I \propto (T_N - T)^{2\beta}$, which yields $T_N = 9(1)$ K and $\beta = 0.37(4)$. (c) A-type antiferromagnetic order in MnBi_2Se_4 with in-plane Mn moments. For simplicity, only Mn atoms within the unit cell of 3 SLs are shown.

The ordered spin moment direction of the Mn ions in vdW MnBi_2Se_4 below T_N can be inferred from representational analysis [44], the photon polarization dependence, as well as the calculation of the magnetic structure factor from the RSXS data. The magnetic representation of the crystallographic site of Mn in vdW MnBi_2Se_4 can be decomposed in terms of the irreducible representations (IRs) [44], with a propagation vector $(0, 0, 1.5)$ (Table I) [45]: $\Gamma_{\text{Mag}} = 1\Gamma_3^1 + 1\Gamma_5^2$, where Γ_3 is a one-dimensional IR with magnetic moments pointing parallel to the c axis (magnetic space group $R\bar{1}\bar{3}c$) and Γ_5 is a two-dimensional IR with basis vectors lying in the ab plane (magnetic space group C_c2/c or C_c2/m). The solution from Γ_3 can be excluded from the following reasoning.

TABLE I. Magnetic symmetry analysis of the vdW MnBi_2Se_4 . Basis vectors (BVs) for the space group $R\bar{3}m$ with the propagation vector $(0, 0, 1.5)$. The decomposition of the magnetic representation for the Mn site is $\Gamma_{\text{Mag}} = 1\Gamma_3^1 + 1\Gamma_5^2$.

IR	BV	atom	BV components					
			$m_{\parallel a}$	$m_{\parallel b}$	$m_{\parallel c}$	$im_{\parallel a}$	$im_{\parallel b}$	$im_{\parallel c}$
Γ_3	ψ_1	1	0	0	1	0	0	0
Γ_5	ψ_2	1	0	1	0	0	0	0
	ψ_3	1	2	1	0	0	0	0

Experimentally, the magnetic peak intensity at the \mathbf{Q}_0 peak position with π -pol incoming x-rays is larger than that of σ -pol x-rays (Fig. 2). This means $I_\pi > I_\sigma$, which can be more specifically written as

$$\left| \sum_j e^{i\mathbf{Q}_0 \cdot \mathbf{r}_j} \mathbf{k}_i \cdot \mathbf{m}_j \right|^2 + \left| \sum_j e^{i\mathbf{Q}_0 \cdot \mathbf{r}_j} \mathbf{e}_\sigma \cdot \mathbf{m}_j \right|^2 > \left| \sum_j e^{i\mathbf{Q}_0 \cdot \mathbf{r}_j} \mathbf{k}_f \cdot \mathbf{m}_j \right|^2, \quad (4)$$

where \mathbf{k}_i and \mathbf{k}_f are the unit vectors along the incoming and outgoing photon wave vector directions, respectively. If the magnetic moments are pointing along the lattice c direction, then for any given \mathbf{m}_j , $\mathbf{e}_\sigma \cdot \mathbf{m}_j = 0$ and $\mathbf{k}_i \cdot \mathbf{m}_j = \mathbf{k}_f \cdot \mathbf{m}_j$, because $\mathbf{m}_j \parallel c$ is perpendicular to the \mathbf{e}_σ direction and bisects the $-\mathbf{k}_i$ and \mathbf{k}_f vectors. This directly leads to $I_\pi = I_\sigma$. Therefore, the experimentally established $I_\pi > I_\sigma$ does not support an Ising moment direction in vdW MnBi_2Se_4 . A similar analysis can be applied to the in-plane spin configuration, which results in $I_{\pi\sigma'} = I_{\sigma\pi'} = I_\sigma$. In this case, $I_{\pi\pi'}$ is typically nonzero because $\mathbf{e}_\sigma \cdot \mathbf{m}_j \neq 0$ (unless in the unique configuration $\mathbf{e}_\sigma \parallel \mathbf{m}_j$), and the magnetic domains equivalently rotated by 120° coexist. Therefore, $I_\pi = I_{\pi\sigma'} + I_{\sigma\pi'} > I_\sigma$ is naturally satisfied with the in-plane moment scenario.

Alternatively, by assuming an out-of-plane spin moment direction, the magnetic structure factor at any Bragg peak reflection along the L direction will be zero, which is exactly the case in the vdW material MnBi_2Te_4 [42,43]. From the above arguments, including the analysis of the magnetic symmetry and the RSXS data, an A-type AFM order with an easy-plane anisotropy in vdW MnBi_2Se_4 is established, as depicted in Fig. 4(c). This is consistent with the magnetization measurements.

III. DISCUSSION

Our work implies the AFM coupled nature in a 13 nm thick vdW MnBi_2Se_4 thin film below $T_N = 9(1)$ K, with intralayer ferromagnetic couplings and interlayer antiferromagnetic couplings. This is in good agreement with density functional theory (DFT) calculations for layered MnBi_2Se_4 [18,19]. The reported hysteresis behavior from the previous magnetization measurement is likely resulting from uncompensated layers [22], which display ferromagnetism due to the strong intralayer ferromagnetic exchange couplings. In addition, the scattering study of the MnBi_2Se_4 thin film disproves claims that the observed magnetism is simply due to some Mn atoms randomly doping the Bi_2Se_3 thin films, which give rise to weak ferromagnetism [46,47].

It should be noted that the in-plane anisotropy established in layered MnBi_2Se_4 by RSXS is not fully consistent with the DFT calculation, which predicts an Ising moment direction [18,19]. This discrepancy can be resolved by considering both the ligand p orbital spin-orbit coupling effect and the magnetic dipole-dipole interactions [22,48–50]. The Mn^{2+} spin state in MnBi_2Te_4 is confirmed from the neutron diffraction measurements, which indicate an ordered magnetic moment $4.9(1) \mu_B/\text{Mn}$ and a $S = \frac{5}{2}$ magnetic state with nearly quenched orbital angular momentum ($L \approx 0$) [51]. However, magnetic

exchange anisotropy can be induced by the ligand p spin-orbit coupling through the super-exchange mechanism [48,49]. Because of the increased atomic number from Se to Te, a larger ligand spin-orbit coupling is expected, resulting from the further extension of the Te p orbitals. This explains the in-plane metallic behavior and a larger $T_N \approx 24$ K in MnBi_2Te_4 [11], while more insulating behavior [22] and a smaller $T_N \approx 9$ K are observed in MnBi_2Se_4 thin film samples. Therefore, a weakened perpendicular magnetization is expected in MnBi_2Se_4 , compared to in MnBi_2Te_4 . On the other hand, the magnetic shape anisotropy resulting from the magnetic dipole-dipole interactions usually supports an in-plane moment configuration. Consequently, because of the smaller magnetic exchange anisotropy resulting from the weaker super-exchange couplings and the magnetic shape anisotropy energy scale in layered MnBi_2Se_4 , the spins are lying within the ab plane, instead of the predicted Ising moment picture.

It is worth mentioning that our heuristic model for the spin direction requires a more quantitative theoretical calculation to underpin the solution between C_c2/c and C_c2/m . Nevertheless, the in-plane spin moment direction in vdW MnBi_2Se_4 , in contrast to the Ising moments in other magnetic topological insulators such as MnBi_2Te_4 , MnSb_2Te_4 , and $\text{Mn}_2\text{Bi}_2\text{Te}_5$ [9–12,51–53], provides an alternative route toward novel topological states (including Weyl line nodes) related to symmetry breaking by magnetic order [16,18,54].

IV. CONCLUSION

In summary, we successfully investigate the intrinsic magnetism in the quasi-2D vdW magnetic topological insulator

MnBi_2Se_4 stabilized via the MBE technique under nonequilibrium conditions. Through a resonant soft x-ray scattering study, an A-type antiferromagnetic order is demonstrated in a 10-SL MnBi_2Se_4 thin film, with a Néel temperature $T_N = 9(1)$ K. The thickness of the sample (~ 13 nm) is nicely determined by the Kiessig fringes. The magnetic order in layered MnBi_2Se_4 is confirmed through the temperature, energy, and polarization dependence of the (0, 0, 0.5) Bragg peak. In addition, the in-plane magnetic anisotropy is readily confirmed by the magnetic symmetry analysis and the polarization dependent study of the magnetic Bragg peak. Compared to other magnetic topological insulators with Ising moments, the alternative spin structure in vdW MnBi_2Se_4 might be useful for realizing new topological states.

ACKNOWLEDGMENTS

Work at the University of California, Berkeley and the Lawrence Berkeley National Laboratory was funded by the U.S. Department of Energy, Office of Science, Office of Basic Energy Sciences, Materials Sciences and Engineering Division under Contract No. DE-AC02-05-CH11231 within the Quantum Materials Program (KC2202). Work at UC San Diego was supported by the National Science Foundation under Grant No. DMR-2145080. Work at Ohio State was funded by AFOSR MURI 2D MAGIC Grant No. FA9550-19-1-0390 and U.S. Department of Energy, Office of Science, Basic Energy Sciences Grant No. DE-SC0016379. We thank HZB for the allocation of synchrotron radiation beam time. A.F. was supported by the Research Corporation for Science Advancement via the Cottrell Scholar Award (27551) and the CIFAR Azrieli Global Scholars program.

-
- [1] F. D. M. Haldane, Model for a quantum Hall effect without landau levels: Condensed-matter realization of the “Parity Anomaly”, *Phys. Rev. Lett.* **61**, 2015 (1988).
- [2] A. M. Essin, J. E. Moore, and D. Vanderbilt, Magnetoelectric polarizability and axion electrodynamics in crystalline insulators, *Phys. Rev. Lett.* **102**, 146805 (2009).
- [3] R. Li, J. Wang, X.-L. Qi, and S.-C. Zhang, Dynamical axion field in topological magnetic insulators, *Nat. Phys.* **6**, 284 (2010).
- [4] R. S. K. Mong, A. M. Essin, and J. E. Moore, Antiferromagnetic topological insulators, *Phys. Rev. B* **81**, 245209 (2010).
- [5] M. Z. Hasan and C. L. Kane, *Colloquium*: Topological insulators, *Rev. Mod. Phys.* **82**, 3045 (2010).
- [6] X.-L. Qi and S.-C. Zhang, Topological insulators and superconductors, *Rev. Mod. Phys.* **83**, 1057 (2011).
- [7] Y. Tokura, K. Yasuda, and A. Tsukazaki, Magnetic topological insulators, *Nat. Rev. Phys.* **1**, 126 (2019).
- [8] C.-Z. Chang, J. Zhang, X. Feng, J. Shen, Z. Zhang, M. Guo, K. Li, Y. Ou, P. Wei, L.-L. Wang, Z.-Q. Ji, Y. Feng, S. Ji, X. Chen, J. Jia, X. Dai, Z. Fang, S.-C. Zhang, K. He, Y. Wang *et al.*, Experimental observation of the quantum anomalous Hall effect in a magnetic topological insulator, *Science* **340**, 167 (2013).
- [9] J. Li, Y. Li, S. Du, Z. Wang, B.-L. Gu, S.-C. Zhang, K. He, W. Duan, and Y. Xu, Intrinsic magnetic topological insulators in van der Waals layered MnBi_2Te_4 -family materials, *Sci. Adv.* **5**, eaaw5685 (2019).
- [10] Y. Gong, J. Guo, J. Li, K. Zhu, M. Liao, X. Liu, Q. Zhang, L. Gu, L. Tang, X. Feng *et al.*, Experimental realization of an intrinsic magnetic topological insulator, *Chin. Phys. Lett.* **36**, 076801 (2019).
- [11] M. M. Otrokov, I. I. Klimovskikh, H. Bentmann, D. Estyunin, A. Zeugner, Z. S. Aliev, S. Gaß, A. Wolter, A. Koroleva, A. M. Shikin *et al.*, Prediction and observation of an antiferromagnetic topological insulator, *Nature (London)* **576**, 416 (2019).
- [12] M. M. Otrokov, I. P. Rusinov, M. Blanco-Rey, M. Hoffmann, A. Y. Vyazovskaya, S. V. Ereemeev, A. Ernst, P. M. Echenique, A. Arnau, and E. V. Chulkov, Unique thickness-dependent properties of the van der Waals interlayer antiferromagnet MnBi_2Te_4 films, *Phys. Rev. Lett.* **122**, 107202 (2019).
- [13] D. Zhang, M. Shi, T. Zhu, D. Xing, H. Zhang, and J. Wang, Topological axion states in the magnetic insulator MnBi_2Te_4 with the quantized magnetoelectric effect, *Phys. Rev. Lett.* **122**, 206401 (2019).
- [14] C. Liu, Y. Wang, H. Li, Y. Wu, Y. Li, J. Li, K. He, Y. Xu, J. Zhang, and Y. Wang, Robust axion insulator and Chern insulator phases in a two-dimensional antiferromagnetic topological insulator, *Nat. Mater.* **19**, 522 (2020).

- [15] Y. Deng, Y. Yu, M. Z. Shi, Z. Guo, Z. Xu, J. Wang, X. H. Chen, and Y. Zhang, Quantum anomalous Hall effect in intrinsic magnetic topological insulator MnBi_2Te_4 , *Science* **367**, 895 (2020).
- [16] B. A. Bernevig, C. Felser, and H. Beidenkopf, Progress and prospects in magnetic topological materials, *Nature (London)* **603**, 41 (2022).
- [17] C.-Z. Chang, C.-X. Liu, and A. H. MacDonald, *Colloquium: Quantum anomalous Hall effect*, *Rev. Mod. Phys.* **95**, 011002 (2023).
- [18] S. Chowdhury, K. F. Garrity, and F. Tavazza, Prediction of Weyl semimetal and antiferromagnetic topological insulator phases in Bi_2MnSe_4 , *npj Comput. Mater.* **5**, 33 (2019).
- [19] H. Zhang, W. Yang, Y. Wang, and X. Xu, Tunable topological states in layered magnetic materials of MnSb_2Te_4 , MnBi_2Se_4 , and MnSb_2Se_4 , *Phys. Rev. B* **103**, 094433 (2021).
- [20] S. Lee, E. Fischer, J. Czerniak, and N. Nagasundaram, Synthesis and structure of two phases with both extended and point defects: $\text{Mn}_{1-x}\text{Bi}_{2+y}\text{S}_4$ and $\text{Mn}_{1-x}\text{Bi}_{2+y}\text{Se}_4$, *J. Alloys Compd.* **197**, 1 (1993).
- [21] C. Nowka, M. Gellesch, J. E. H. Borrero, S. Partzsch, C. Wuttke, F. Steckel, C. Hess, A. U. Wolter, L. T. C. Bohorquez, B. Büchner *et al.*, Chemical vapor transport and characterization of MnBi_2Se_4 , *J. Cryst. Growth* **459**, 81 (2017).
- [22] T. Zhu, A. J. Bishop, T. Zhou, M. Zhu, D. J. O'Hara, A. A. Baker, S. Cheng, R. C. Walko, J. J. Repicky, T. Liu *et al.*, Synthesis, magnetic properties, and electronic structure of magnetic topological insulator MnBi_2Se_4 , *Nano Lett.* **21**, 5083 (2021).
- [23] R. C. Walko, T. Zhu, A. J. Bishop, R. K. Kawakami, and J. A. Gupta, Scanning tunneling microscopy study of the antiferromagnetic topological insulator MnBi_2Se_4 , *Physica E* **143**, 115391 (2022).
- [24] M. Blume, Magnetic scattering of x rays (invited), *J. Appl. Phys.* **57**, 3615 (1985).
- [25] J. P. Hannon, G. T. Trammell, M. Blume, and D. Gibbs, X-ray resonance exchange scattering, *Phys. Rev. Lett.* **61**, 1245 (1988).
- [26] J. Fink, E. Schierle, E. Weschke, and J. Geck, Resonant elastic soft x-ray scattering, *Rep. Prog. Phys.* **76**, 056502 (2013).
- [27] R. Comin and A. Damascelli, Resonant x-ray scattering studies of charge order in cuprates, *Annu. Rev. Condens. Matter Phys.* **7**, 369 (2016).
- [28] L. Paolasini, Resonant and magnetic X-ray diffraction by polarized synchrotron radiation, *École thématique de la Société Française de la Neutronique* **13**, 03002 (2014).
- [29] G. Decher, Fuzzy nanoassemblies: Toward layered polymeric multicomposites, *Science* **277**, 1232 (1997).
- [30] F. Katmis, V. Lauter, F. S. Nogueira, B. A. Assaf, M. E. Jamer, P. Wei, B. Satpati, J. W. Freeland, I. Eremin, D. Heiman *et al.*, A high-temperature ferromagnetic topological insulating phase by proximity coupling, *Nature (London)* **533**, 513 (2016).
- [31] X. Chen, E. Schierle, Y. He, M. Vranas, J. W. Freeland, J. L. McChesney, R. Ramesh, R. J. Birgeneau, and A. Frano, Antiferromagnetic order in Co-doped Fe_5GeTe_2 probed by resonant magnetic x-ray scattering, *Phys. Rev. Mater.* **6**, 094404 (2022).
- [32] S. B. Wilkins, P. D. Spencer, P. D. Hatton, S. P. Collins, M. D. Roper, D. Prabhakaran, and A. T. Boothroyd, Direct observation of orbital ordering in $\text{La}_{0.5}\text{Sr}_{1.5}\text{MnO}_4$ using soft x-ray diffraction, *Phys. Rev. Lett.* **91**, 167205 (2003).
- [33] Y. W. Windsor, S. W. Huang, Y. Hu, L. Rettig, A. Alberca, K. Shimamoto, V. Scagnoli, T. Lippert, C. W. Schneider, and U. Staub, Multiferroic properties of $o\text{-LuMnO}_3$ controlled by b -axis strain, *Phys. Rev. Lett.* **113**, 167202 (2014).
- [34] H. Padmanabhan, V. A. Stoica, P. K. Kim, M. Poore, T. Yang, X. Shen, A. H. Reid, M.-F. Lin, S. Park, J. Yang *et al.*, Large exchange coupling between localized spins and topological bands in MnBi_2Te_4 , *Adv. Mater.*, **34** 2202841 (2022).
- [35] A. Biffin, R. D. Johnson, S. Choi, F. Freund, S. Manni, A. Bombardi, P. Manuel, P. Gegenwart, and R. Coldea, Unconventional magnetic order on the hyperhoneycomb Kitaev lattice in $\beta\text{-Li}_2\text{IrO}_3$: Full solution via magnetic resonant x-ray diffraction, *Phys. Rev. B* **90**, 205116 (2014).
- [36] S. Boseggia, H. Walker, J. Vale, R. Springell, Z. Feng, R. Perry, M. M. Sala, H. M. Rønnow, S. Collins, and D. F. McMorrow, Locking of iridium magnetic moments to the correlated rotation of oxygen octahedra in Sr_2IrO_4 revealed by x-ray resonant scattering, *J. Phys.: Condens. Matter* **25**, 422202 (2013).
- [37] See Supplemental Material at <http://link.aps.org/supplemental/10.1103/PhysRevB.109.184418> for additional data of the rocking scans and longitudinal scans near the charge and magnetic peaks.
- [38] R. Guida and J. Zinn-Justin, Critical exponents of the N -vector model, *J. Phys. A: Math. Gen.* **31**, 8103 (1998).
- [39] A. Pelissetto and E. Vicari, Critical phenomena and renormalization-group theory, *Phys. Rep.* **368**, 549 (2002).
- [40] R. J. Birgeneau, J. Als-Nielsen, and G. Shirane, Critical behavior of pure and site-random two-dimensional antiferromagnets, *Phys. Rev. B* **16**, 280 (1977).
- [41] X. Chen, Y. He, S. Wu, Y. Song, D. Yuan, E. Bourret-Courchesne, J. P. C. Ruff, Z. Islam, A. Frano, and R. J. Birgeneau, Structural and magnetic transitions in the planar antiferromagnet $\text{Ba}_4\text{Ir}_3\text{O}_{10}$, *Phys. Rev. B* **103**, 224420 (2021).
- [42] L. Ding, C. Hu, F. Ye, E. Feng, N. Ni, and H. Cao, Crystal and magnetic structures of magnetic topological insulators MnBi_2Te_4 and MnBi_4Te_7 , *Phys. Rev. B* **101**, 020412 (2020).
- [43] J.-Q. Yan, Q. Zhang, T. Heitmann, Z. Huang, K. Y. Chen, J.-G. Cheng, W. Wu, D. Vaknin, B. C. Sales, and R. J. McQueeney, Crystal growth and magnetic structure of MnBi_2Te_4 , *Phys. Rev. Mater.* **3**, 064202 (2019).
- [44] A. S. Wills, A new protocol for the determination of magnetic structures using simulated annealing and representational analysis (SARA h), *Phys. B: Condens. Matter* **276-278**, 680 (2000).
- [45] Here, a full lattice constant $c = 3c_{\text{SL}}$ is used for the representational analysis. Therefore, the propagating vector is $3\mathbf{Q}_0 = (0, 0, 1.5)$.
- [46] D. Zhang, A. Richardella, D. W. Rench, S.-Y. Xu, A. Kandala, T. C. Flanagan, H. Beidenkopf, A. L. Yeats, B. B. Buckley, P. V. Klimov, D. D. Awschalom, A. Yazdani, P. Schiffer, M. Z. Hasan, and N. Samarth, Interplay between ferromagnetism, surface states, and quantum corrections in a magnetically doped topological insulator, *Phys. Rev. B* **86**, 205127 (2012).
- [47] H. J. von Bardeleben, J. L. Cantin, D. M. Zhang, A. Richardella, D. W. Rench, N. Samarth, and J. A. Borchers, Ferromagnetism in Bi_2Se_3 :Mn epitaxial layers, *Phys. Rev. B* **88**, 075149 (2013).
- [48] J. L. Lado and J. Fernández-Rossier, On the origin of magnetic anisotropy in two dimensional CrI_3 , *2D Mater.* **4**, 035002 (2017).

- [49] D.-H. Kim, K. Kim, K.-T. Ko, J. H. Seo, J. S. Kim, T.-H. Jang, Y. Kim, J.-Y. Kim, S.-W. Cheong, and J.-H. Park, Giant magnetic anisotropy induced by ligand LS coupling in layered Cr compounds, *Phys. Rev. Lett.* **122**, 207201 (2019).
- [50] F. Xue, Y. Hou, Z. Wang, and R. Wu, Two-dimensional ferromagnetic van der Waals CrCl_3 monolayer with enhanced anisotropy and Curie temperature, *Phys. Rev. B* **100**, 224429 (2019).
- [51] L. Ding, C. Hu, E. Feng, C. Jiang, I. A. Kibalin, A. Gukasov, M. Chi, N. Ni, and H. Cao, Neutron diffraction study of magnetism in van der waals layered $\text{MnBi}_{2n}\text{Te}_{3n+1}$, *J. Phys. D* **54**, 174003 (2021).
- [52] B. Chen, F. Fei, D. Zhang, B. Zhang, W. Liu, S. Zhang, P. Wang, B. Wei, Y. Zhang, Z. Zuo *et al.*, Intrinsic magnetic topological insulator phases in the Sb doped MnBi_2Te_4 bulks and thin flakes, *Nat. Commun.* **10**, 4469 (2019).
- [53] T. Murakami, Y. Nambu, T. Koretsune, G. Xiangyu, T. Yamamoto, C. M. Brown, and H. Kageyama, Realization of interlayer ferromagnetic interaction in MnSb_2Te_4 toward the magnetic Weyl semimetal state, *Phys. Rev. B* **100**, 195103 (2019).
- [54] J. Li and R. Wu, Electrically tunable topological phase transition in van der Waals heterostructures, *Nano Lett.* **23**, 2173 (2023).